




Article

Evaluation of VEGETATION and PROBA-V Phenology Using PhenoCam and Eddy Covariance Data

Kevin Bórnez ^{1,2,*}, Andrew D. Richardson ^{3,4}, Alexandre Verger ^{1,2} , Adrià Descals ^{1,2}  and Josep Peñuelas ^{1,2} 

¹ CREAM, Cerdanyola del Vallès, 08193 Bellaterra, Catalonia, Spain; verger@creaf.uab.cat (A.V.); a.descals@creaf.uab.cat (A.D.); Josep.Penuelas@uab.cat (J.P.)

² CSIC, Global Ecology Unit CREAM-CSIC-UAB, 08193 Bellaterra, Catalonia, Spain

³ Center for Ecosystem Science and Society, Northern Arizona University, Flagstaff, AZ 86011, USA; Andrew.Richardson@nau.edu

⁴ School of Informatics, Computing and Cyber Systems, Northern Arizona University, Flagstaff, AZ 86011, USA

* Correspondence: k.bornez@creaf.uab.cat

Received: 17 August 2020; Accepted: 16 September 2020; Published: 19 September 2020



Abstract: High-quality retrieval of land surface phenology (LSP) is increasingly important for understanding the effects of climate change on ecosystem function and biosphere–atmosphere interactions. We analyzed four state-of-the-art phenology methods: threshold, logistic-function, moving-average and first derivative based approaches, and retrieved LSP in the North Hemisphere for the period 1999–2017 from Copernicus Global Land Service (CGLS) SPOT-VEGETATION and PROBA-V leaf area index (LAI) 1 km V2.0 time series. We validated the LSP estimates with near-surface PhenoCam and eddy covariance FLUXNET data over 80 sites of deciduous forests. Results showed a strong correlation ($R^2 > 0.7$) between the satellite LSP and ground-based observations from both PhenoCam and FLUXNET for the timing of the start (SoS) and $R^2 > 0.5$ for the end of season (EoS). The threshold-based method performed the best with a root mean square error of ~9 d with PhenoCam and ~7 d with FLUXNET for the timing of SoS (30th percentile of the annual amplitude), and ~12 d and ~10 d, respectively, for the timing of EoS (40th percentile).

Keywords: Land-surface phenology; SPOT-VEGETATION; PROBA-V; leaf area index; PhenoCam; FLUXNET

1. Introduction

The study of vegetation phenology and its patterns on a global scale have become more important since the late twentieth century for analyzing the effects of climate change [1,2]. Remote sensing is a useful tool for characterizing land surface phenology (LSP) [3] and global changes of vegetation [4–6]. De Beurs et al. [7] analyzed a broad range of statistical methods designed to extract phenological metrics from satellite time series based on threshold percentiles [8–10], moving averages [11], first derivatives [12,13], smoothing functions [14] and fitted models [15].

Most literature on LSP has focused on the use of time series of vegetation indices mainly derived from MODIS data [6,16,17]. In previous studies, we showed the added value of using Copernicus Global Land Service (CGLS) leaf area index (LAI) time series derived from VEGETATION and PROBA-V data [10,18]. Bórnez et al. [18] found that the phenological metrics extracted from the CGLS LAI Version 2 (V2) time series agreed best with the available human-based ground observations of phenological transition dates for deciduous broadleaf forest in Europe (PEP727) and United States

of America (USA-NPN) as compared to other biophysical variables and NDVI vegetation index or previous version V1 of the CGLS products.

Validating LSP is challenging due, in part, to the differences in the definition of satellite metrics and ground phenophases [13,19]. Volunteer observers have traditionally collected data for the timing of specific phenophases of individual plants [20]. Human observations of phenology, however, are not uniform and may induce uncertainties, despite efforts to establish protocols for monitoring phenophases [21–23].

Near-surface remote sensing using conventional red-green-blue (RGB) digital cameras provides an alternative to human observations to monitor vegetation phenology [24–28] because of their low cost, ease of set up and capacity to collect detailed spectral information at high temporal frequencies [29] of individual plants, species or canopies [30] across broad spatial scales [31–33]. PhenoCam [34] is a network of digital cameras that currently includes >600 site-years of imagery, with high-quality and high temporal resolution providing data of vegetation phenology. Deciduous broadleaved forests (68 sites) are the dominant vegetation type within the PhenoCam Network [35], and the focus of this study. A growing number of studies have compared transition dates derived from the PhenoCam time series of green chromatic coordinates (GCC) with satellite phenological metrics derived mainly from MODIS data [29,36–38].

Continuous flux measurements from eddy covariance technique also started to be used as a new perspective for estimating LSP at the landscape level [5,39–43]. The flux measurements sites are organized as a confederation of regional networks around the world, called FLUXNET [44]. Until the last updated of February 2020, the most recent dataset produced was the FLUXNET2015 dataset [44] which includes data from 212 sites [45].

In this study, we build on our previous work [18] and take advantage now of PhenoCam and FLUXNET capability of continuous monitoring of vegetation seasonal growth at very high temporal resolution, with data every 30 minutes [26,46–49]. This allows a more robust and accurate comparison with LSP derived from satellite time series avoiding problems related to the differences in the definition of phenology metrics. We evaluated four methods for estimating phenology: the threshold method based on percentiles [10], the derivative method [12], the autoregressive moving-average method [11] and the logistic-function method [50]. These methods were applied both to satellite CGLS LAI V2 time series and ground observations from PhenoCam GCC and eddy covariance flux towers over deciduous forests to assess the accuracy of LSP retrievals.

2. Materials and Methods

2.1. Study Area

The study was conducted over the North Hemisphere in pixels classified as deciduous forests or mixed vegetation according to the annual C3S Global Land Cover for the year 2018 [51]. The validation was done over PhenoCam sites distributed across North America and one in Europe, and FLUXNET towers sites both in North America and Europe and one in Japan. We selected only deciduous forests sites with at least 2 years of available observations. This resulted in 64 sites from PhenoCam, and 16 towers of FLUXNET covering a broad range of latitudes (30–60°N) and elevations (1–1870 m a.s.l.) (Figure 1 and Table S1).

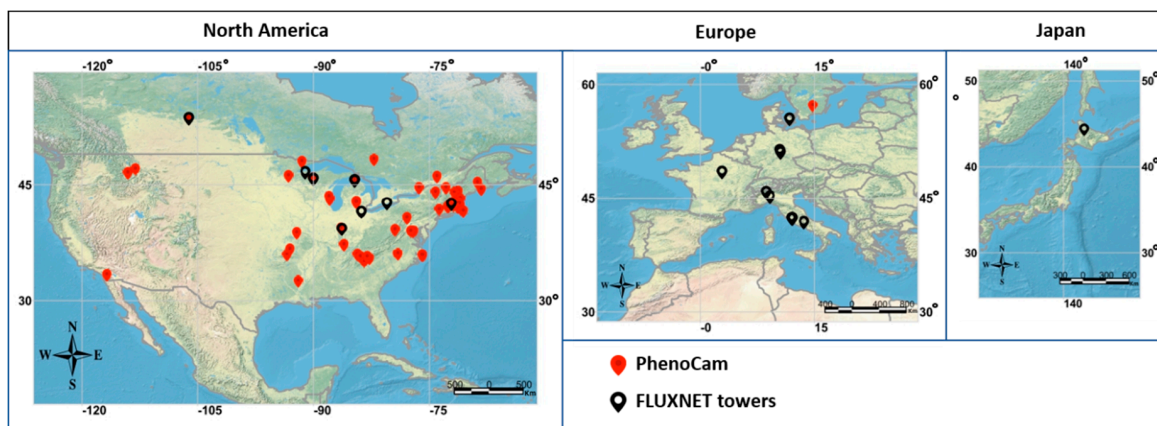


Figure 1. Locations of the selected PhenoCam sites (red) and FLUXNET towers (black) over deciduous forests.

2.2. Satellite Data: CGLS LAI

We used Copernicus land surface products (CGLS LAI V2) derived from SPOT-VEGETATION (1999–2013) and PROBA-V (2014–2017) data. The spatial resolution is 1 km and the temporal frequency is 10 d [52].

The algorithm for LAI V2 product [53,54] capitalizes on the development and validation of already existing products (CYCLOPES version 3.1 and MODIS collection 5 products) and the use of neural networks [55]. The inputs of the neural networks are daily top of the canopy reflectances from VEGETATION and PROBA-V in the red, near-infrared and shortwave infrared spectral bands and the sun and view geometry. A multi-step procedure for filtering, temporal smoothing, gap-filling and compositing is then applied to the daily estimates to generate the final 10 d products [53].

2.3. PhenoCam Data

We used PhenoCam Dataset V1.0 [34,56]. It provides digital images every 30 min. In each image, a “region of interest” was defined manually based on the dominant vegetation type in the camera field of view [35] (Figure 2). The size of the ROI typically ranges from ~50 to ~500 m² [34,35]. The green chromatic coordinate (GCC) index [35] was calculated from the red (R), green (G) and blue (B) digital numbers (DN) as:

$$G_{cc} = \frac{GDN}{RDN + GDN + BDN} \quad (1)$$

We used the 90th percentile G_{CC} value and 1 d high quality composites to avoid noise from variations in meteorological, atmospheric or illumination conditions [57]. We manually filtered the poor-quality G_{CC} observations and then gap-filled the missing data with a locally weighted scatter-plot smoother (lowess)-based filter [35].

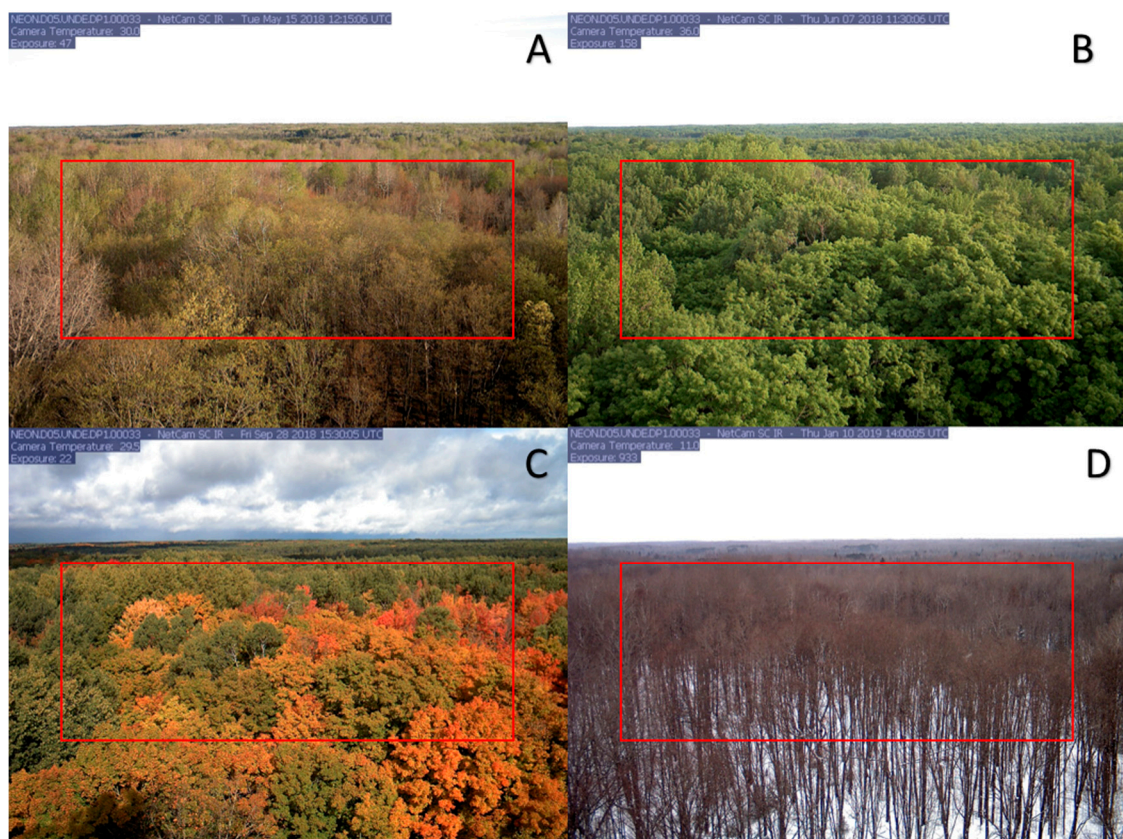


Figure 2. PhenoCam images captured in (A) spring, (B) summer, (C) autumn and (D) winter over the NEON.D05.UNDE.DP1.00033 site (46.23°N, 89.54°W). The red rectangle indicates the borders of the selected region of interest.

2.4. FLUXNET Data

We used FLUXNET 2015 collection of gross primary production (GPP) flux data over 16 forest tower sites (Figure 1) for the period 2003–2014 (110 site-years) [44]. We used the daily GPP ($\text{g C m}^{-2} \text{d}^{-1}$) derived from half-hourly eddy covariance flux measurements using the night time based approach [58,59]. We smoothed the series of the daily GPP by using a Savitzky–Golay filter based on a second degree polynomial and a 30-day smoothing window [60–62].

2.5. Methods for Estimating Vegetation Phenology

We tested four methods for estimating phenology (Table 1 and Figure 3, [18]) from satellite (CGLS LAI time series) and ground-based data (PhenoCam GCC, FLUXNET GPP) (e.g., Figure S2 in Supplementary Materials). The phenological metrics are the timing of the start of the growing season (SoS), the end of the growing season (EoS) and the length of the growing season (LoS). LoS was estimated as the length of time between the EoS and the SoS. The CGLS LAI 10 d time series were linearly interpolated at daily steps before phenological retrieval.

Table 1. Description of the evaluated methods for the extraction of phenology metrics.

Method.	Reference	Principles and Parameters
Threshold based on percentiles	Verger et al. [10]	SoS is defined as the first day of the year (DoY) when the vegetation variable exceeds a particular threshold. EoS is defined as the DoY when an index descends below a threshold. We established dynamic thresholds per pixel based on a percentile (10th, 25th, 30th, 40th and 50th) of the annual amplitude
Logistic function	Zhang et al. [50]	SoS is defined as the DoY with the first local maximum rate of change in the curvature of a logistic function fitted to the time series. EoS is defined as the DoY with the first local minimum rate of change in the curvature
First derivative	Tateishi and Ebata. [12]	SoS is defined as the DoY of the maximum increase (maximum first derivative) in the curve. EoS is defined as the DoY of the maximum decrease in the curve
Autoregressive moving average	Reed et al. [11]	A moving average is first computed at a given time lag (we tested 10–50 d and selected a 30 d time lag). SoS and EoS are then defined as the DoY when the moving-average curves cross the original time series of the vegetation index

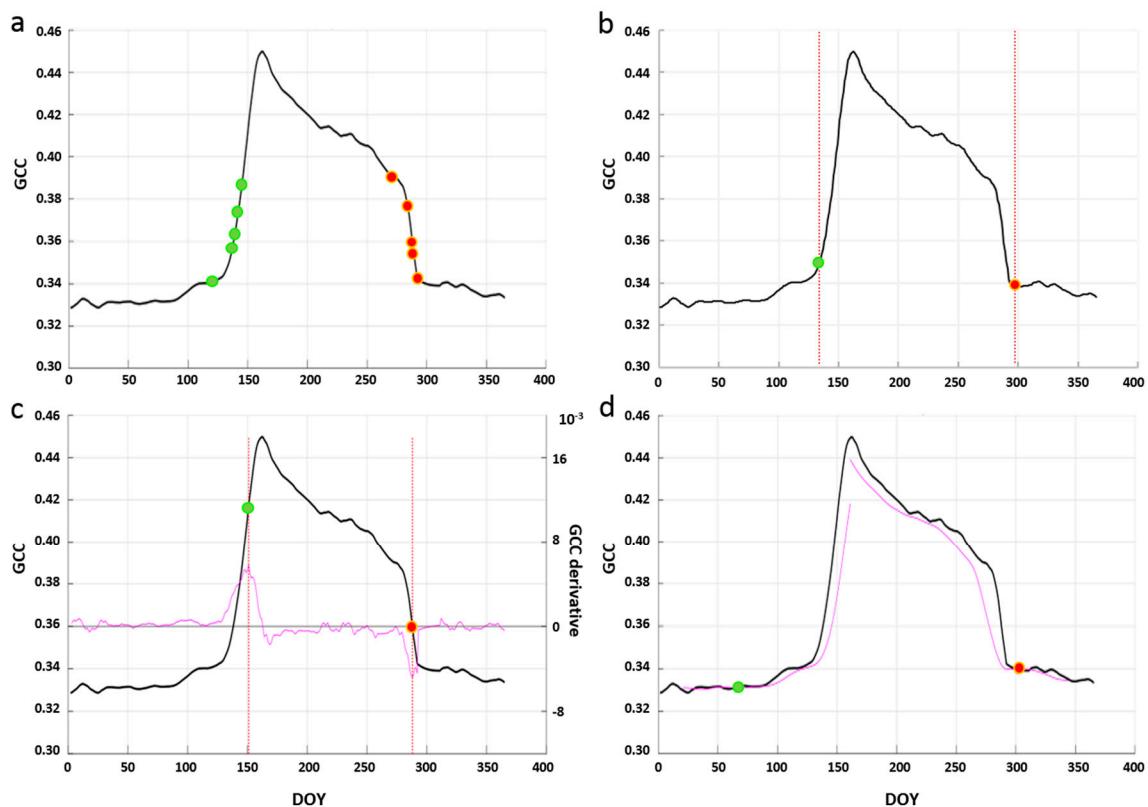


Figure 3. Illustration of the threshold (a), logistic-function (b), derivative (c) and moving-average (d) phenological extraction methods applied to PhenoCam G_{CC} time series of Acadia site (44.37°N , 68.26°W) for 2014. The green and red points correspond to SoS and EoS, respectively. The different points in panel a correspond to the percentiles 10th, 25th, 30th, 40th and 50th. The purple line corresponds to the first derivative in c, and to the moving average in d.

2.6. Validation Approach

The LSP derived from VEGETATION and PROBA-V LAI V2 time series was compared with the LSP estimates using ground data from PhenoCam and FLUXNET when the same phenological extraction method was applied (Section 3.1). The statistical metrics used for assessing the performance are the root mean square error (RMSE), the mean error (bias); the coefficient of determination (R^2), slope and intercept of the Reduced Major Axis regression (RMA). Further the spatial patterns and latitudinal gradients of LSP estimates were assessed in Section 3.2. We used RStudio for the statistical analysis, Google Earth Engine (GEE, <https://earthengine.google.org>) for the retrieval of LSP over the North Hemisphere, and ESRI ArcGIS 10.5 and gvSIG-desktop-2.3.1 for the graphs and maps.

3. Results

3.1. Comparison of Satellite and Ground Phenologies

The coefficient of determination, R^2 , between the satellite- and ground-based estimates from PhenoCam and FLUXNET phenology ranges from 0.01 to 0.81 ($p < 0.001$) (Table 2). The threshold-based method provided the best performances. The 30th percentile of annual amplitude was the best threshold for the SoS (RMSE < 9 d, bias < 2 d and $R^2 = 0.74$ with $p < 0.001$ for CGLS LAI V2 estimates compared to PhenoCam; and RMSE < 7 d, bias < 4 d and $R^2 = 0.81$ with $p < 0.001$ when compared to FLUXNET) and the 40th percentile for the EoS (RMSE = 12 d, bias < 1 d and $R^2 = 0.51$ with $p < 0.001$ compared to PhenoCam; RMSE < 10 d, bias < 5 d and $R^2 = 0.53$ with $p < 0.001$ compared to FLUXNET).

Table 2. Statistics of the comparison between the SoS and EoS dates retrieved using the LAI, GCC, and GPP estimates for the four methods: thresholds, logistic function, derivative and moving average. * indicates significant correlations at $p < 0.05$; **, significant correlations at $p < 0.001$. The bold type highlights the best method. Evaluation over the 64 PhenoCam sites (356 samples (sites \times years)) and 16 FLUXNET towers (110 samples (sites \times years)) over deciduous forests in the North Hemisphere (Figure 1).

Metric	Validation	Method	RMSE	BIAS	R^2	Slope	Intercept
SoS	PhenoCam	Threshold (10th percentile)	17.80	-0.53	0.29	1.07	-8.57
		Threshold (25th percentile)	9.92	1.29	0.61 **	1.02	-8.57
		Threshold (30th percentile)	8.82	1.96	0.74 **	1.01	0.7
		Threshold (40th percentile)	9.05	2.61	0.67 **	1.02	-0.39
		Threshold (50th percentile)	9.45	3.74	0.65 **	1.00	2.98
		Logistic function	10.79	1.21	0.58 **	0.99	1.18
		Derivative	19.27	2.40	0.18	0.93	11.12
		Moving average	15.49	0.48	0.42 *	1.24	-30.9
SoS	FLUXNET	Threshold (10th percentile)	16.50	3.54	0.31	0.90	14.03
		Threshold (25th percentile)	7.91	-2.08	0.7 **	1.00	-2.91
		Threshold (30th percentile)	6.77	-3.56	0.81 **	1.03	-8.02
		Threshold (40th percentile)	7.21	-3.91	0.80 **	0.99	-3.24
		Threshold (50th percentile)	8.42	-5.65	0.77 **	1.04	-11.8
		Logistic function	8.05	-0.42	0.69 **	0.94	6.06
		Derivative	23.63	-14.31	0.19	0.61	41.66
		Moving average	16.09	1.99	0.37 *	0.79	30.13
EoS	PhenoCam	Threshold (10th percentile)	15.33	5.59	0.33 *	0.88	40.86
		Threshold (25th percentile)	12.90	2.27	0.45 *	0.91	28.12
		Threshold (30th percentile)	13.49	1.36	0.39 *	0.92	22.75
		Threshold (40th percentile)	12.07	0.65	0.51 **	0.95	13.51
		Threshold (50th percentile)	29.31	7.23	0.09	0.49	142.16
		Logistic function	17.64	-0.93	0.26	0.82	52.52
		Derivative	50.74	-1.50	0.03	0.33	179.59
		Moving average	27.40	2.15	0.01	1.46	-140.06
EoS	FLUXNET	Threshold (10th percentile)	10.84	6.25	0.5 **	1.00	5.93
		Threshold (25th percentile)	9.80	5.29	0.55 **	1.04	-5.93
		Threshold (30th percentile)	9.99	4.90	0.44 *	1.06	-12.38
		Threshold (40th percentile)	9.67	4.67	0.53 **	1.18	-46.54
		Threshold (50th percentile)	17.39	9.88	0.18	0.76	71.9
		Logistic function	10.26	2.97	0.41 *	1.10	-26.47
		Derivative	48.06	32.40	0.01	-0.09	289.18
		Moving average	31.50	-14.30	0.04	0.53	114.78

Figures 4 and 5 show the scatter plots of the comparison of satellite and ground-based SoS and EoS retrievals for the four methods. The points were very close to the 1:1 line using the percentile and logistic-function methods while the derivative and moving-average methods produced worse results with more widely dispersed points, especially for the timing of EoS.

The satellite SoS (Figure 4, Figure 5 and Figure S1) retrieved with threshold and logistic-function methods showed RMSE < 11 d and bias < 2 d compared to PhenoCam, and RMSE < 8 d and bias < 4 d with FLUXNET (Table 2). Higher discrepancies for the SoS were found with the derivative and moving-average methods: RMSE of 19 d and 15 d, and bias of 2 d and < 1 d, respectively using PhenoCam estimates, and RMSE of 24 d and 16 d, and bias of -14 d and 2 d, respectively with FLUXNET estimates (Table 2).

The EoS can be also robustly estimated using remote sensing observations (Figure 4, Figure 5 and Figure S1) although we observed a degradation of performances for all the methods for the estimation of the EoS as compared to the SoS: higher dispersion of points, higher RMSE and lower correlation for EoS (Table 2). The EoS estimates from satellite time series of LAI agreed the best with GCC and GPP derived phenology metrics using the threshold method followed by the logistic function: RMSE of 12 d and 18 d, respectively, and biases < 1 d compared to PhenoCam, and RMSE of 10 d and bias < 5 d with FLUXNET (Table 2). The performance highly decreased for the derivative and moving average

methods with RMSE of 50 d and 27 d, respectively, compared to PhenoCam, and RMSE of 48 d and 31 d with FLUXNET, and no significant correlation ($R^2 < 0.2$) (Table 2).

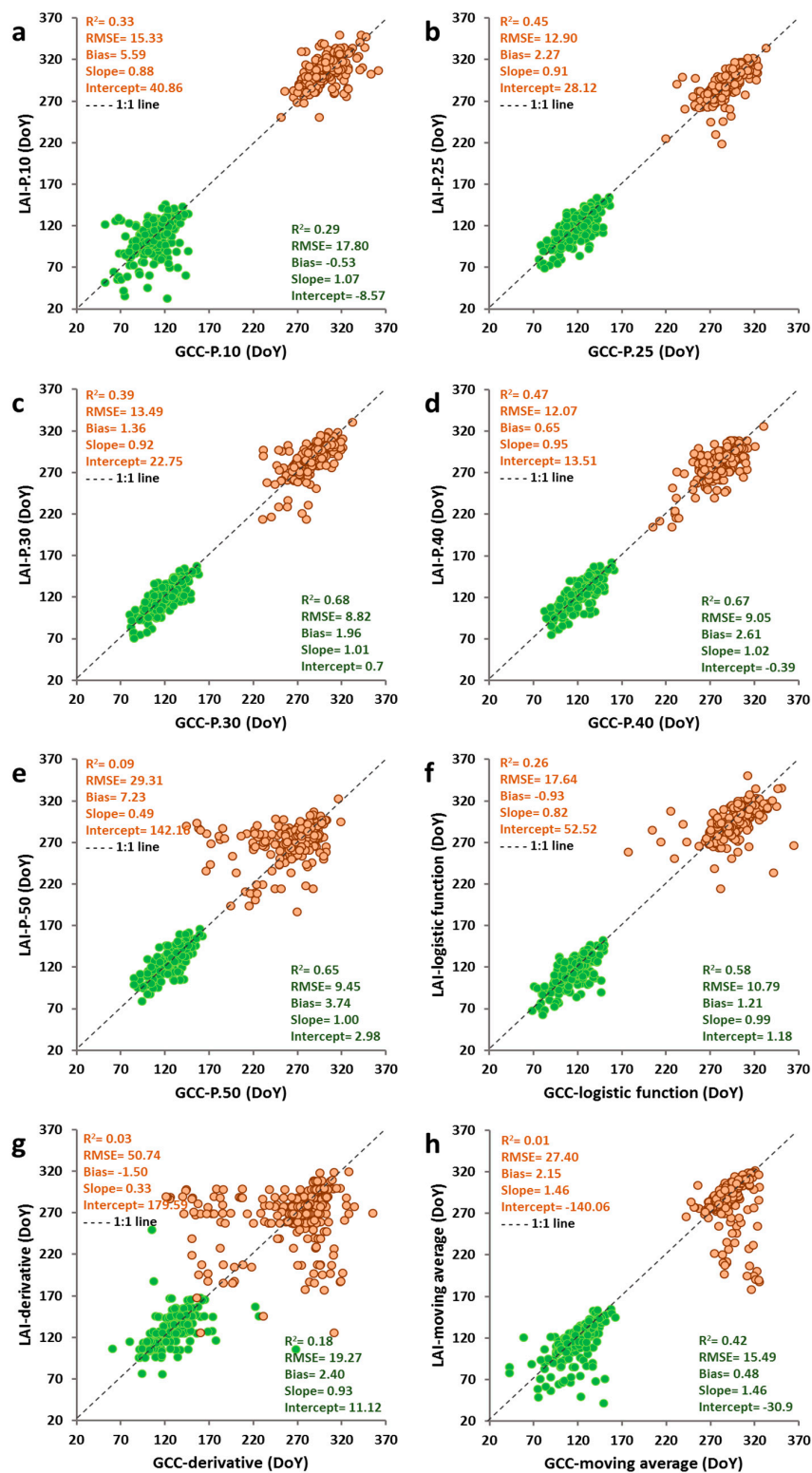


Figure 4. Scatterplots for SoS (in green) and EoS (in orange) estimated from CGLS LAI V2 and PhenoCam GCC time series by the threshold (10th (a), 25th (b), 30th (c), 40th (d) and 50th (e) percentiles of LAI amplitude), logistic-function (f), derivative (g) and moving-average (h) methods. Statistics of the comparison are presented in Table 2.

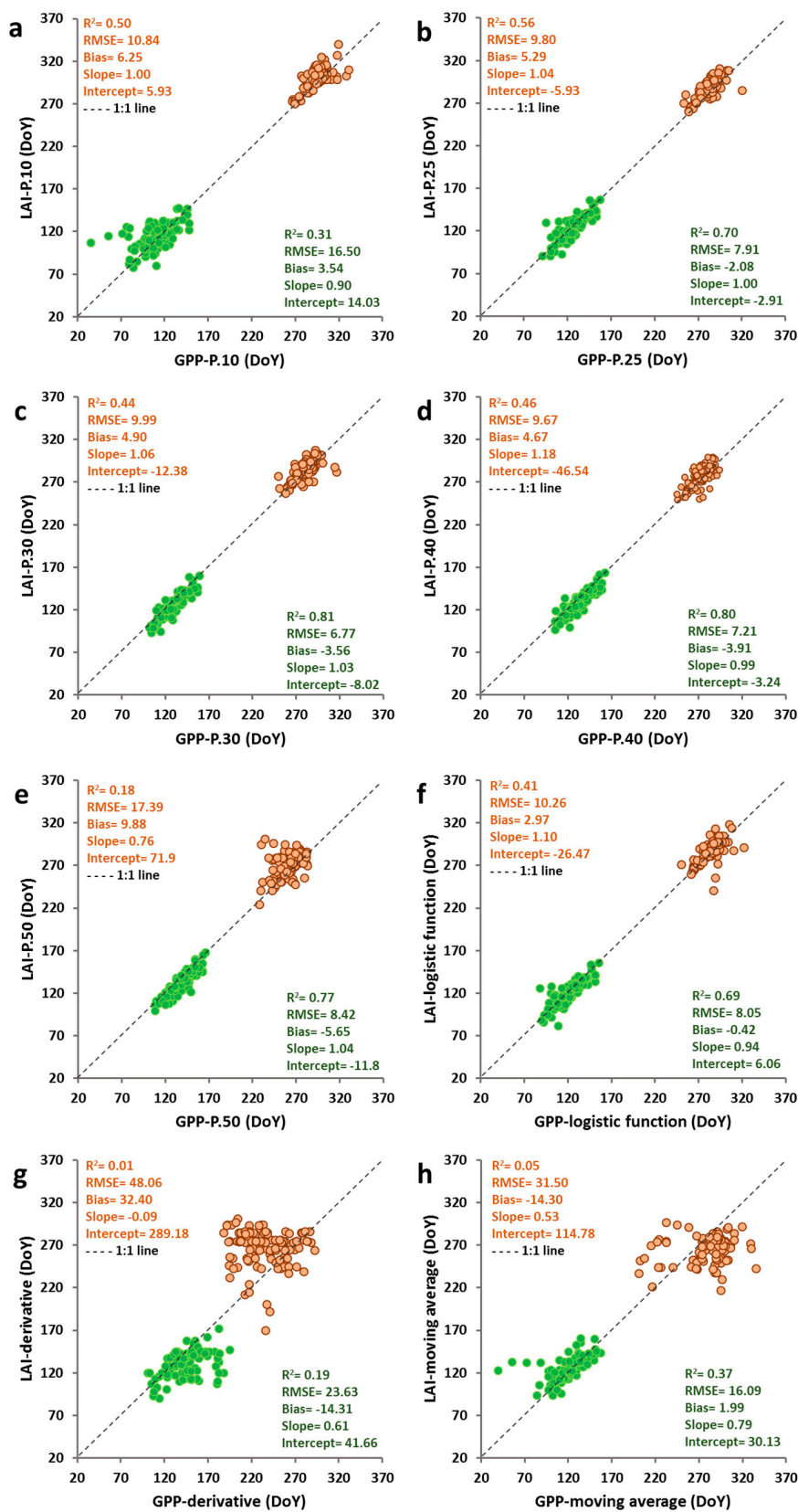


Figure 5. Scatterplots for SoS (in green) and EoS (in orange) estimated from CGLS LAI V2 and FLUXNET GPP time series by the threshold (10th (a), 25th (b), 30th (c), 40th (d) and 50th (e) percentiles of LAI amplitude, logistic-function (f), derivative (g) and moving-average (h) methods. Statistics of the comparison are presented in Table 2.

3.2. Latitudinal Gradients of Satellite and Ground-Based Phenology

Figure S3 shows the spatial distribution of the GCLS LAI phenological estimates (SoS, EoS, and LoS) from 2000 to 2017 over the North Hemisphere using the threshold method. The length of the vegetation cycles regularly decreases from 220 days to 80 days when latitude increases from temperate to boreal regions. The SoS ranges widely from late march in the south to approximately mid-July in the north. The SoS is slightly earlier in central Europe than in North America for the same latitude. The EoS date ranges from early August to December.

The latitudinal patterns of the timings of SoS and EoS derived from CGLS LAI V2 (Figure S3) and PhenoCam GCC over deciduous forests from 30°N to 53°N in North America showed a very good agreement with a gradual decrease in the length of growing season of approximately five days per degree of latitude which resulted from symmetric variations of 2.5 days per degree of latitude in the start and end of season (Figure 6). We found a correlation R^2 of 0.92 for the timing of SoS and 0.88 for the EoS when comparing the average satellite and PhenoCam phenology per latitude.

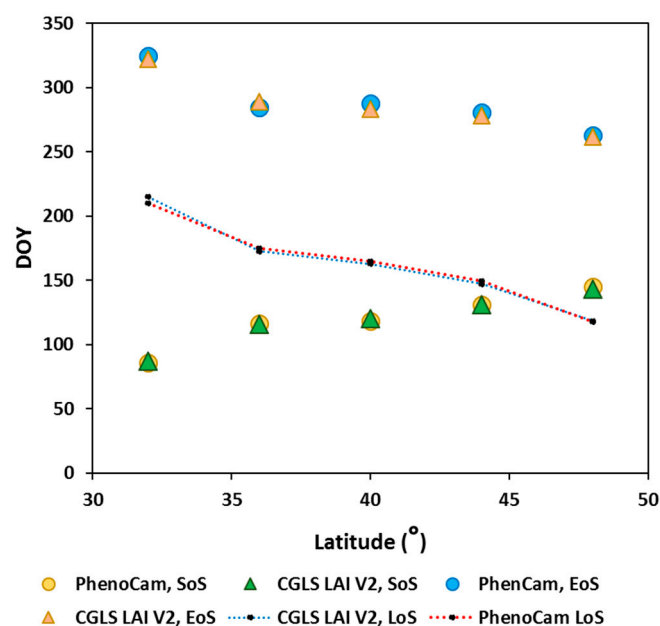


Figure 6. Latitudinal gradients of average phenological metrics for the start (SoS), end (EoS) and length of season (LoS) extracted from CGLS LAI V2 and PhenoCam GCC time series over the PhenoCam deciduous sites in North America (Figure 1). Data was aggregated in five groups of latitude, taking into account the number of sites: 30–34°N, 34–38°N, 38–42°N, 42–46°N and 46–53°N.

4. Discussion

We assessed the agreement of the phenological metrics derived from satellite LAI (CGLS LAI V2 from VEGETATION and PROBA-V time series, 1999–2017) with those derived from PhenoCam (GCC) and FLUXNET flux towers (GPP) across 80 sites of deciduous forests mainly located in North America and Europe. The agreement between satellite and ground-based estimates depends on the method used to extract the transition dates. We compared four phenology methods: thresholds based on percentiles of the annual amplitude [10], first derivatives [12], autoregressive moving average [11] and a logistic function fitting approach [50]. Thresholds and logistic function resulted the most robust methods and the phenological metrics extracted from CGLS LAI V2 time series were strongly correlated with those derived from PhenoCam GCC and FLUXNET GPP. On the contrary the derivative and moving average methods showed higher discrepancies between satellite and ground estimates specifically for the timing of the EoS.

The threshold-based method performed the best in terms of accuracy of satellite estimates for the timing of the SoS and EoS: RMSE ~ 9 d and bias < 2 d for the SoS, RMSE ~ 12 d and bias < 1 d for the EoS, and correlation of $R^2 \sim 0.7$ compared to PhenoCam data; and RMSE < 7 d and bias < 4 d for the SoS, RMSE < 10 d and bias < 5 d for the EoS, and correlation $R^2 \sim 0.8$ compared to FLUXNET data. In both PhenoCam and FLUXNET comparison, the 30th percentile of the annual amplitude provided the best performances for the timing of the SoS and the 40th percentile for the EoS, confirming our previous findings [10,18]. These thresholds slightly outperformed 10th, 25th and 50th percentiles of the amplitude as proposed in PhenoCam Dataset V1.0 for the extraction of the phenological transition dates [35]. For the sites with concomitant measurements from the 3 sources of data: satellite LAI, PhenoCam GCC and FLUXNET GPP, we observed that the phenology derived from LAI V2 using percentiles 30 and 40 accurately reproduce the interannual variation of the SoS and EoS and usually provides an intermediate solution between PhenoCam and FLUXNET estimates with differences lower than 10 days (Figure 7). The latitudinal gradient in the northern hemisphere of the CGLS LAI V2 phenophases highly agree with PhenoCam observations with an advance (delay) of 2.5 days per degree of latitude from low to high latitudes in response to the South-North gradient of temperature and photoperiod [63,64]. These results are comparable to other studies [65]. The spatial variability in phenophases can be explained not only by the difference in climatic patterns but also by the elevation and soil conditions [66].

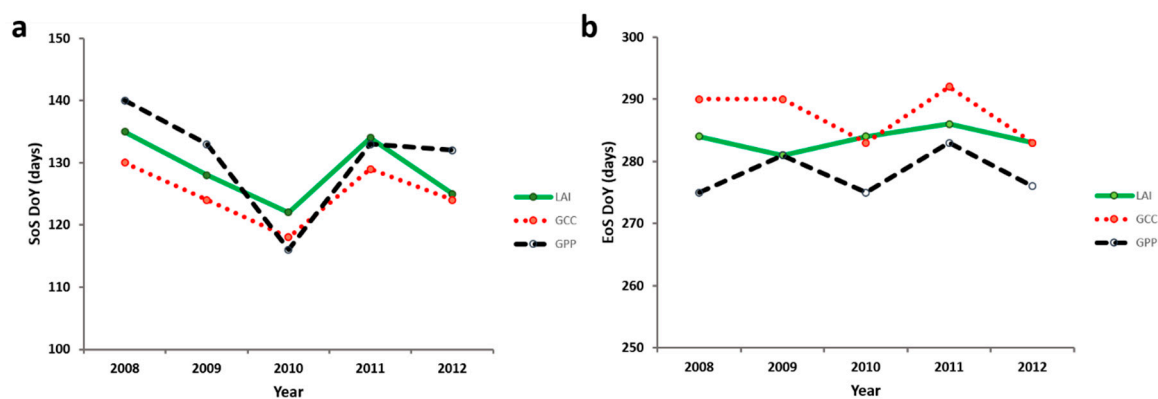


Figure 7. Interannual variation of the (a) start of the growing season (SoS), and (b) end of season (EoS) estimated from the CGLS LAI V2, PhenoCam GCC and FLUXNET GPP with the threshold method (percentile 30 for the timing of SoS, and percentile 40 for the timing of EoS) over the Harvard Forest (Latitude 42.54° , Longitude -72.17°).

Detecting phenology from carbon flux and PhenoCam data also faces some challenges [26,46]. The flux measurements are potentially $\sim 20\%$ biased due to the lack of energy balance closure, instrument response time, pathlength averaging and incomplete measurement of nocturnal CO_2 exchange [46,67,68] which can lead uncertainties in phenology estimates. However, these errors are difficult to quantify and correct [26]. Furthermore, for some FLUXNET sites, there are substantial data gaps due to instrument malfunction or bad data quality [46]. In these cases, the gap-filling may lead to uncertainty in GPP time series and, consequently, in the phenological estimates [69].

The scale difference between ~ 1 km VEGETATION and PROBA-V satellite pixels and the deca-/hectometric footprints of PhenoCam cameras and flux towers may introduce some difficulties for the comparison. This is partially minimized because our validation is limited to deciduous forests which tend to form large patches of the same vegetation type, reducing the influence of mixed or border pixels [26,70,71]. The mixed signal due to multi-canopy layers may also introduce confounding effects since the understorey may have a different phenological cycle [70]. The emergence of forest understorey is interpreted in both ground-based and satellite observations as an increase in the greening signal.

The agreement between the PhenoCam, FLUXNET and remotely sensed phenological metrics showed generally a higher accuracy for SoS than EoS, consistent with previous studies [18,29,64,72–75].

Differences in the structure, ecophysiology and dynamics of the vegetation canopy at the start and end of the growing season [37] may partially explain this. The phenological dynamics for the timing of EoS tend to vary with species, age, dispersion and homogeneity, and can also differ across the same species, with differences of up to two weeks within the same ROI [26,43,71,76,77]. Further studies will use high resolution satellite data from Sentinel-2 to mitigate these issues and capture the spatial variability of EoS [78]. Note, however, that monitoring EoS is affected by the intrinsic uncertainties of satellite remote sensing at northern latitudes in autumn: atmospheric effects, snow and poor illumination conditions [79].

5. Conclusions

Phenological data from PhenoCam, FLUXNET and satellite remotely sensed data have become a broad resource for analyzing the relationships between global change and vegetation [29,35]. The network of PhenoCam webcams and eddy covariance towers cover only small areas around the camera or flux tower [40,80]. Satellite imagery has the advantage of providing continuous spatio-temporal coverage at the global scale. Near-surface digital cameras and flux towers have nevertheless become a good tool for characterizing local phenology and validate satellite estimates [26,37,57,81]. The high temporal frequency of PhenoCam and flux measurements provide continuous time series for applying the same phenology extraction methods to ground and satellite time series. This way, we avoid some of the issues identified in our previous research [18] related to the differences in the definition of satellite phenology metrics and ground phenophases when PEP725 and USA-NPN data were used for the validation (e.g.; the representativity and spatial distribution of the data as well as the gaps in the time series of ground measurements).

Results validate the land surface phenology estimated from CGLS LAI V2 time series, as well as the robustness of PhenoCam and FLUXNET data to analyze vegetation phenology. This study has put bounds on the uncertainty in satellite-derived phenological transitions, which should allow to analyze changes in the phenological distribution pattern and serve as a starting point for other studies that characterize anomalies and trends over vegetation phenology, as well as its possible relationship with changes in the climate pattern as a result of climate change.

Supplementary Materials: The following are available online at <http://www.mdpi.com/2072-4292/12/18/3077/s1>, Figure S1: “Boxplots of the bias errors of satellite-based minus the near-surface estimates of SoS (a) and EoS (b) over the 64 PhenoCam sites (a,b), and the 16 FLUXNET towers (c,d) for the four extraction methods: threshold method (the 30th percentile of annual amplitude for the SoS (a, c) and the 40th percentile for the EoS (b, d)), the logistic-function, first derivatives and moving-average. An elongated boxplot indicates a larger dispersion of the average bias”. Figure S2: “Time series of CGLS LAI, PhenoCam GCC and FLUXNET GPP for the Harvard Forest site (42.5378N, -72.1715O) over the 2008-2012 period”. Figure S3: “Maps of average SoS (a), EoS (b) and LoS (c) derived from CGLS LAI V2 time series (1999-2017) using the threshold method (30th percentile of annual LAI amplitude for SoS and 40th percentile for EoS). The maps show the estimated phenology in deciduous or mixed forest based on the annual C3S Global Land Cover for the year 2018 (<http://maps.elie.ucl.ac.be/CCI/viewer/download.php>). The continental areas in white are lakes, deserts, agricultural areas and evergreen forests. The phenology was not computed for pixels with very limited seasonality: when the annual amplitude ((max (LAI) – min (LAI)) was lower than the 30% of the median value in the time series ($0.3 * LAI_{50th}$). For pixels with multiple growing seasons, we computed the phenological metrics for the growing season having the highest LAI amplitude”. Table S1: “Characteristics of PhenoCam [38] and FLUXNET fluxnet.fluxdata.org [44] sites. The Start date and End date indicates the period of available data. MAT is mean annual temperature and MAP is mean annual precipitation based on climate data are from WorldClim. Primary and secondary vegetation types are as follows: AG = agriculture; DB = deciduous broadleaf; DN = deciduous needleleaf; EB = evergreen broadleaf; EN = evergreen needleleaf; GR = grassland; MX = mixed vegetation (generally EN/DN, DB/EN, or DB/EB); SH = shrubs; TN = tundra (includes sedges, lichens, mosses, etc.); WL = wetland”.

Author Contributions: Conceptualization, K.B., A.V., J.P. and A.D.R.; methodology, A.V., J.P. and K.B.; software, A.D. and K.B.; validation, K.B. and A.D.; formal analysis, K.B.; investigation, K.B.; resources, A.D.R., K.B., A.V. and A.D.; data curation, K.B., A.D. and A.V.; writing—original draft preparation, K.B.; writing—review and editing, A.V., J.P., A.D.R., A.D. and K.B.; visualization, K.B. and A.V.; supervision, A.V., J.P. and A.D.R.; project administration, J.P. and A.V.; funding acquisition, K.B., A.V. and J.P. All authors have read and agreed to the published version of the manuscript.

Funding: This research received no external funding.

Acknowledgments: The LAI products were generated by the Global Land Service of Copernicus, the Earth Observation program of the European Commission. The products are based on 1 km SPOT-VEGETATION data (copyright CNES and distribution by VITO NV) and on PROBA-V 1 km data (copyright Belgian Science Policy and distribution by VITO NV). This research was supported by an FPU grant (Formación del Profesorado Universitario) from the Spanish Ministry of Education and Professional Training to the first author (FPU2015-04798), the Copernicus Global Land Service (CGLOPS-1, 199494-JRC), the Spanish Government grant PID2019-110521GB-I00, the Catalan Government grant SGR 2017-1005 and the European Research Council Synergy grant ERC-2013-SyG-610028 IMBALANCE-P. We thank our many collaborators, including members of the PhenoCam project team as well as site PIs and technicians, for their efforts in support of PhenoCam. A.D.R. acknowledges for PhenoCam from the Northeastern States Research Cooperative, NSF (EF-1065029, EF-1702697), Department of Energy (DE-SC0016011), and United States Geological Survey (G10AP00129, G16AC00224).

Conflicts of Interest: The authors declare no conflict of interest.

References

- Chimielewski, F.M.; Rotz, T. Response of tree phenology to climate change across Europe. *Agr. For. Meteorol.* **2001**, *108*, 101–112. [[CrossRef](#)]
- Peñuelas, J.; Filella, I. Responses to a warming world. *Science* **2001**, *294*, 793–795. [[CrossRef](#)] [[PubMed](#)]
- Baumann, M.; Özdoğan, M.; Richardson, A.D.; Radeloff, V.C. Phenology from Landsat when data is scarce: Using MODIS and Dynamic Time-Warping to combine multi-year Landsat imagery to derive annual phenology curves. *Int. J. Appl. Earth Obs. Geoinf.* **2017**, *54*, 72–83. [[CrossRef](#)]
- White, K.; Pontius, J.; Schaberg, P. Remote sensing of spring phenology in northeastern forests: A comparison of methods, field metrics and sources of uncertainty. *Remote Sens. Environ.* **2014**, *148*, 97–107. [[CrossRef](#)]
- Wu, C.; Chen, J.M. Deriving a new phenological indicator of interannual net carbon exchange in contrasting boreal deciduous and evergreen forests. *Ecol. Indic.* **2013**, *24*, 113–119. [[CrossRef](#)]
- Zhang, X.; Jayavelu, S.; Liu, L.; Friedl, M.A.; Henebry, G.M.; Liu, Y.; Schaaf, C.B.; Richardson, A.D.; Gray, J. Evaluation of land surface phenology from VIIRS data using time series of PhenoCam imagery. *Agric. For. Meteorol.* **2018**, *256*, 137–149. [[CrossRef](#)]
- De Beurs, K.; Henebry, G. Spatio-temporal statistical methods for modelling land surface phenology. In *Phenological Research: Methods for Environmental and Climate Change Analysis*; Hudson, I., Keatley, M., Eds.; Springer: Dordrecht, The Netherlands, 2010; pp. 177–208.
- Reed, B.C.; White, M.; & Brown, J.F. Remote sensing phenology. In *Phenology: An integrative Environmental Science*; Schwartz, M.D., Ed.; Kluwer Academic Publishing: Dordrecht, The Netherlands, 2003; pp. 365–381.
- Atzberger, C.; Klisch, A.; Mattiuzzi, M.; Vuolo, F. Phenological metrics derived over the European continent from NDVI3g data and MODIS time series. *Remote Sens.* **2013**, *6*, 257–284. [[CrossRef](#)]
- Verger, A.; Filella, I.; Baret, F.; Peñuelas, J. Vegetation baseline phenology from kilometeric global LAI satellite products. *Remote Sens. Environ.* **2016**, *178*, 1–14. [[CrossRef](#)]
- Reed, B.C.; Brown, J.F.; Vanderzee, D.; Loveland, T.R.; Merchant, J.W.; Ohlen, D.O. Measuring phenological variability from satellite imagery. *J. Veg. Sci.* **1994**, *5*, 703–714. [[CrossRef](#)]
- Tateishi, R.; Ebata, M. Analysis of phenological change patterns using 1982–2000 Advanced Very High-Resolution Radiometer (AVHRR) data. *Int. J. Remote Sens.* **2004**, *25*, 2287–2300. [[CrossRef](#)]
- White, M.A.; de Beurs, K.M.; Digan, K.; Inouye, D.W.; Richardson, A.D.; Jensen, O.P.; O’Keefe, J.; Zhang, G.; Nemani, R.R.; Van Leeuwen, W.J.D.; et al. Intercomparison, interpretation, and assessment of spring phenology in North America estimated from remote sensing for 1982–2006. *Global Change Biol.* **2009**, *15*, 2335–2359. [[CrossRef](#)]
- Piao, S.; Friedlingstein, P.; Ciais, P.; Zhou, L.; Chen, A. Effect of climate and CO₂ changes on the greening of the Northern Hemisphere over the past two decades. *Geophys. Res. Lett.* **2006**, *33*, 23402. [[CrossRef](#)]
- De Beurs, K.M.; Henebry, G.M. Land surface phenology and temperature variation in the International Geosphere-Biosphere Program high-latitude transects. *Glob. Chang. Biol.* **2005**, *11*, 779–790. [[CrossRef](#)]
- Zhang, X.; Friedl, M.A.; Schaaf, C. Global vegetation phenology from Moderate Resolution Imaging Spectroradiometer (MODIS): Evaluation of global patterns and comparison with in situ measurements. *J. Geophys. Res. Space Phys.* **2006**, *111*. [[CrossRef](#)]
- Ganguly, S.; Friedl, M.A.; Tan, B.; Zhang, X.; Verma, M. Land surface phenology from MODIS: Characterization of the Collection 5 global land cover dynamics product. *Remote Sens. Environ.* **2010**, *114*, 1805–1816. [[CrossRef](#)]

18. Bórnez-Mejías, K.; Descals, A.; Verger, A.; Peñuelas, J. Land surface phenology from VEGETATION and PROBA-V data. Assessment over deciduous forests. *Int. J. Appl. Earth Obs. Geoinf.* **2020**, *84*, 101974. [[CrossRef](#)]
19. Schwartz, M.D.; Hanes, J.M. Intercomparing multiple measures of the onset of spring in eastern North America. *Int. J. Clim.* **2009**, *30*, 1614–1626. [[CrossRef](#)]
20. Menzel, A. Phenology: Its importance to the global change community. *Clim. Chang.* **2002**, *54*, 379–385. [[CrossRef](#)]
21. Denny, E.; Gerst, K.L.; Miller-Rushing, A.J.; Tierney, G.L.; Crimmins, T.M.; Enquist, C.A.F.; Guertin, P.; Rosemartin, A.H.; Schwartz, M.D.; Thomas, K.A.; et al. Standardized phenology monitoring methods to track plant and animal activity for science and resource management applications. *Int. J. Biometeorol.* **2014**, *58*, 591–601. [[CrossRef](#)]
22. Templ, B.; Koch, E.; Bolmgren, K.; Ungersböck, M.; Paul, A.; Scheifinger, H.; Rutishauser, T.; Busto, M.; Chmielewski, F.-M.; Hajkova, L.; et al. Pan European Phenological database (PEP725): A single point of access for European data. *Int. J. Biometeorol.* **2018**, *62*, 1109–1113. [[CrossRef](#)]
23. Tierney, G.; Mitchell, B.; Miller-Rushing, A.; Katz, J.; Denny, E.; Brauer, C.; Donovan, T.; Richardson, A.; Toomey, M.; Kozlowski, A.; et al. *Phenology Monitoring Protocol: Northeast Temperate Network*; Technical Report No. NPS/NETN//NRR-2013/681; National Park Service: Fort Collins, CO, USA, 2013; p. 254.
24. Jacobs, N.; Burgin, W.; Fridrich, N.; Abrams, A.; Miskell, K.; Braswell, B.; Richardson, A.D.; Pless, R. The global network of outdoor webcams: Properties and applications. In Proceedings of the 17th ACM International Conference on Advances in Geographic Information Systems, Seattle, WA, USA, 3–6 November 2009; pp. 111–120. [[CrossRef](#)]
25. Richardson, A.D.; Jenkins, J.P.; Braswell, B.; Hollinger, D.Y.; Ollinger, S.V.; Smith, M.-L. Use of digital webcam images to track spring green-up in a deciduous broadleaf forest. *Oecologia* **2007**, *152*, 323–334. [[CrossRef](#)] [[PubMed](#)]
26. Richardson, A.D.; Braswell, B.; Hollinger, D.Y.; Jenkins, J.P.; Ollinger, S.V. Near-surface remote sensing of spatial and temporal variation in canopy phenology. *Ecol. Appl.* **2009**, *19*, 1417–1428. [[CrossRef](#)] [[PubMed](#)]
27. Hufkens, K.; Basler, D.; Milliman, T.; Melaas, E.K.; Richardson, A.D. An integrated phenology modelling framework in R. *Methods Ecol. Evol.* **2018**, *9*, 1276–1285. [[CrossRef](#)]
28. Keenan, T.F.; Darby, B.; Felts, E.; Sonnentag, O.; Friedl, M.A.; Hufkens, K.; O’Keefe, J.; Klosterman, S.; Munger, J.W.; Toomey, M.; et al. Tracking forest phenology and seasonal physiology using digital repeat photography: A critical assessment. *Ecol. Appl.* **2014**, *24*, 1478–1489. [[CrossRef](#)] [[PubMed](#)]
29. Hufkens, K.; Friedl, M.A.; Keenan, T.F.; Sonnentag, O.; Bailey, A.; O’Keefe, J.; Richardson, A.D. Ecological impacts of a widespread frost event following early spring leaf-out. *Glob. Chang. Biol.* **2012**, *18*, 2365–2377. [[CrossRef](#)]
30. Bater, C.W.; Coops, N.C.; Wulder, M.A.; Nielsen, S.E.; McDermid, G.J.; Stenhouse, G. Design and installation of a camera network across an elevation gradient for habitat assessment. *Instrum. Sci. Technol.* **2011**, *39*, 231–247. [[CrossRef](#)]
31. Brown, T.; Hultine, K.R.; Steltzer, H.; Denny, E.; Denslow, M.; Granados, J.; Henderson, S.; Moore, D.J.P.; Nagai, S.; San Clements, M.; et al. Using phenocams to monitor our changing Earth: Toward a global phenocam network. *Front. Ecol. Environ.* **2016**, *14*, 84–93. [[CrossRef](#)]
32. Laskin, D.N.; McDermid, G.J. Evaluating the level of agreement between human and time-lapse camera observations of understory plant phenology at multiple scales. *Ecol. Informatics* **2016**, *33*, 1–9. [[CrossRef](#)]
33. Morissette, J.T.; Richardson, A.D.; Knapp, A.K.; I Fisher, J.; A Graham, E.; Abatzoglou, J.T.; E Wilson, B.; Breshears, D.D.; Henebry, G.M.; Hanes, J.M.; et al. Tracking the rhythm of the seasons in the face of global change: Phenological research in the 21st century. *Front. Ecol. Environ.* **2009**, *7*, 253–260. [[CrossRef](#)]
34. PhenoCam Dataset v1.0 Used in This Study Is Publicly Available through the ORNL DAAC. Available online: https://daac.ornl.gov/VEGETATION/guides/PhenoCam_V1.html (accessed on 12 July 2020).
35. Richardson, A.D.; Hufkens, K.; Milliman, T.; Aubrecht, D.M.; Chen, M.; Gray, J.M.; Johnston, M.R.; Keenan, T.F.; Klosterman, S.T.; Kosmala, M.; et al. Tracking vegetation phenology across diverse North American biomes using PhenoCam imagery. *Sci. Data* **2018**, *5*, 180028. [[CrossRef](#)]
36. Melaas, E.; Friedl, M.A.; Richardson, A.D. Multiscale modeling of spring phenology across Deciduous Forests in the Eastern United States. *Glob. Chang. Biol.* **2016**, *22*, 792–805. [[CrossRef](#)] [[PubMed](#)]

37. Klosterman, S.T.; Hufkens, K.; Gray, J.M.; Melaas, E.; Sonnentag, O.; LaVine, I.; Mitchell, L.; Norman, R.; Friedl, M.A.; Richardson, A.D. Evaluating remote sensing of deciduous forest phenology at multiple spatial scales using PhenoCam imagery. *Biogeosciences* **2014**, *11*, 4305–4320. [[CrossRef](#)]
38. Richardson, A.D.; Hufkens, K.; Milliman, T.; Frohling, S. Intercomparison of phenological transition dates derived from the PhenoCam Dataset V1.0 and MODIS satellite remote sensing. *Sci. Rep.* **2018**, *8*, 5679. [[CrossRef](#)] [[PubMed](#)]
39. Ahrends, H.; Etzold, S.; Kutsch, W.; Stoeckli, R.; Bruegger, R.; Jeanneret, F.; Wanner, H.; Buchmann, N.; Eugster, W. Tree phenology and carbon dioxide fluxes: Use of digital photography for process-based interpretation at the ecosystem scale. *Clim. Res.* **2009**, *39*, 261–274. [[CrossRef](#)]
40. Gonsamo, A.; Chen, J.M.; Price, D.T.; A Kurz, W.; Wu, C. Land surface phenology from optical satellite measurement and CO₂ eddy covariance technique. *J. Geophys. Res. Space Phys.* **2012**, *117*. [[CrossRef](#)]
41. Gonsamo, A.; Chen, J.; D’Odorico, P. Deriving land surface phenology indicators from CO₂ eddy covariance measurements. *Ecol. Indic.* **2013**, *29*, 203–207. [[CrossRef](#)]
42. Noormets, A.; Chen, J.; Gu, L.; Desai, A.R. The phenology of gross ecosystem productivity and ecosystem respiration in temperate hard-wood and conifer chronosequences. In *Phenology of Ecosystem Processes: Applications in Global Change Research*; Noormets, A., Ed.; Springer: New York, NY, USA, 2009; pp. 58–85.
43. Richardson, A.D.; Black, T.A.; Ciais, P.; Delbart, N.; Friedl, M.A.; Gobron, N.; Hollinger, D.Y.; Kutsch, W.L.; Longdoz, B.; Luyssaert, S.; et al. Influence of spring and autumn phenological transitions on forest ecosystem productivity. *Philos. Trans. R. Soc. B Boil. Sci.* **2010**, *365*, 3227–3246. [[CrossRef](#)]
44. FLUXNET Data. Available online: <http://fluxnet.fluxdata.org/data/fluxnet2015-dataset/> (accessed on 10 July 2020).
45. Joiner, J.; Yoshida, Y.; Zhang, Y.; Duveiller, G.; Jung, M.; Lyapustin, A.; Wang, Y.; Tucker, C.J. Estimation of terrestrial global gross primary production (GPP) with satellite data-driven models and eddy covariance flux data. *Remote Sens.* **2018**, *10*, 1346. [[CrossRef](#)]
46. Hollinger, D.Y.; Richardson, A.D. Uncertainty in eddy covariance measurements and its application to physiological models. *Tree Physiol.* **2005**, *25*, 873–885. [[CrossRef](#)]
47. Xiao, X.; Zhang, Q.; Hollinger, D.; Aber, J.; Moore, B. Modeling gross primary production of an evergreen needleleaf forest using MODIS and climate data. *Ecol. Appl.* **2005**, *15*, 954–969. [[CrossRef](#)]
48. Xiao, X.; Zhang, J.; Yan, H.; Wu, W.; Biradar, C. Land surface phenology. In *Phenology of Ecosystem Processes*; Noormets, A., Ed.; Springer: New York, NY, USA, 2009; pp. 247–270.
49. Yan, D.; Scott, R.; Moore, D.; Biederman, J.; Smith, W. Understanding the relationship between vegetation greenness and productivity across dryland ecosystems through the integration of PhenoCam, satellite, and eddy covariance data. *Remote Sens. Environ.* **2019**, *223*, 50–62. [[CrossRef](#)]
50. Zhang, X.; Friedl, M.A.; Schaaf, C.; Strahler, A.H.; Hodges, J.C.; Gao, F.; Reed, B.C.; Huete, A. Monitoring vegetation phenology using MODIS. *Remote Sens. Environ.* **2003**, *84*, 471–475. [[CrossRef](#)]
51. C3S Global Land Cover Map. Available online: <http://maps.elie.ucl.ac.be/CCI/viewer/download.php> (accessed on 18 July 2020).
52. CGLS LAI V2 Data. Available online: <https://land.copernicus.eu/global/themes/vegetation> (accessed on 8 July 2020).
53. Verger, A.; Baret, F.; Weiss, M. Near Real-Time Vegetation Monitoring at Global Scale. *IEEE J. Sel. Top. Appl. Earth Obs. Remote Sens.* **2014**, *7*, 3473–3481. [[CrossRef](#)]
54. Verger, A.; Baret, F.; Weiss, M. Algorithm Theoretical Basis Document: LAI, FAPAR, FCOVER Collection 1km, Version 2, Issue I1.41. 2019. Available online: https://land.copernicus.eu/global/sites/cgls.vito.be/files/products/CGLOPS1_ATBD_LAI1km-V2_I1.41.pdf (accessed on 10 July 2020).
55. Verger, A.; Baret, F.; Weiss, M. Performances of neural networks for deriving LAI estimates from existing CYCLOPES and MODIS products. *Remote Sens. Environ.* **2008**, *112*, 2789–2803. [[CrossRef](#)]
56. Richardson, A.D.; Milliman, T.; Hufkens, K.; Aubrecht, D.M.I.; Chen, M.; Gray, J.M.; Johnston, M.R.; Keenan, T.; Klosterman, S.T.; Kosmala, M.; et al. *PhenoCam Dataset v1.0: Vegetation Phenology from Digital Camera Imagery, 2000–2015*; ORNL Distributed Active Archive Center: Washington, DC, USA, 2017.
57. Sonnentag, O.; Hufkens, K.; Teshera, C.; Young, A.M.; Fiedl, M.; Braswell, B.H.; Milliman, T.; O’Keefe, J.; Richardson, A.D. Digital repeat photography for phenological research in forest ecosystems. *Agric. For. Meteorol.* **2012**, *152*, 159–177. [[CrossRef](#)]

58. Reichstein, M.; Falge, E.; Baldocchi, D.; Papale, D.; Aubinet, M.; Berbigier, P.; Bernhofer, C.; Buchmann, N.; Gilmanov, T.; Granier, A.; et al. On the separation of net ecosystem exchange into assimilation and ecosystem respiration: Review and improved algorithm. *Glob. Chang. Biol.* **2005**, *11*, 1424–1439. [[CrossRef](#)]
59. Vuichard, N.; Papale, D. Filling the gaps in meteorological continuous data measured at FLUXNET sites with ERA-Interim reanalysis. *Earth Syst. Sci. Data* **2015**, *7*, 157–171. [[CrossRef](#)]
60. Savitzky, A.; Golay, M.J.E. Smoothing and differentiation of data by simplified least squares procedures. *Anal. Chem.* **1964**, *36*, 1627–1639. [[CrossRef](#)]
61. Chen, J.; Jönsson, P.; Tamura, M.; Gu, Z.; Matsushita, B.; Eklundh, L. A simple method for reconstructing a high-quality NDVI time-series data set based on the Savitzky-Golay filter. *Remote Sens. Environ.* **2004**, *91*, 332–344. [[CrossRef](#)]
62. Wu, C.; Peng, D.; Soudani, K.; Siebicke, L.; Gough, C.M.; Arain, M.A.; Bohrer, G.; LaFleur, P.M.; Peichl, M.; Gonsamo, A.; et al. Land surface phenology derived from normalized difference vegetation index (NDVI) at global FLUXNET sites. *Agric. For. Meteorol.* **2017**, *233*, 171–182. [[CrossRef](#)]
63. Schwartz, M.D.; Ahas, R.; Aasa, A. Onset of spring starting earlier across the Northern Hemisphere. *Glob. Change Biol.* **2006**, *12*, 343–351. [[CrossRef](#)]
64. Richardson, A.D.; Keenan, T.F.; Migliavacca, M.; Ryu, Y.; Sonnentag, O.; Toomey, M. Climate change, phenology, and phenological control of vegetation feedbacks to the climate system. *Agric. For. Meteorol.* **2013**, *169*, 156–173. [[CrossRef](#)]
65. Zhang, X.; Friedl, M.A.; Schaaf, C.; Strahler, A.H. Climate controls on vegetation phenological patterns in northern mid- and high latitudes inferred from MODIS data. *Glob. Change Biol.* **2004**, *10*, 1133–1145. [[CrossRef](#)]
66. Rodriguez-Galiano, V.F.; Dash, J.; Atkinson, P.M. Characterising the land surface phenology of Europe using decadal MERIS data. *Remote Sens.* **2015**, *7*, 9390–9409. [[CrossRef](#)]
67. Massman, W.J.; Lee, X. Eddy covariance flux corrections and uncertainties in long-term studies of carbon and energy exchanges. *Agric. For. Meteorol.* **2002**, *113*, 121–144. [[CrossRef](#)]
68. Morgenstern, K.; Black, T.A.; Humphreys, E.; Griffis, T.J.; Drewitt, G.B.; Cai, T.; Nesic, Z.; Spittlehouse, D.L.; Livingston, N.J. Sensitivity and uncertainty of the carbon balance of a Pacific Northwest Douglas-fir forest during an El Niño/La Niña cycle. *Agric. For. Meteorol.* **2004**, *123*, 201–219. [[CrossRef](#)]
69. Baldocchi, D. Assessing the eddy covariance technique for evaluating carbon dioxide exchange rates of ecosystems: Past, present and future. *Glob. Change Biol.* **2003**, *9*, 479–492. [[CrossRef](#)]
70. Ryu, Y.; Lee, G.; Jeon, S.; Song, Y.; Kimm, H. Monitoring multi-layer canopy spring phenology of temperate deciduous and evergreen forests using low-cost spectral sensors. *Remote Sens. Environ.* **2014**, *149*, 227–238. [[CrossRef](#)]
71. Richardson, A.D.; Bailey, A.S.; Denny, E.; Martin, C.W.; O’Keefe, J. Phenology of a northern hardwood forest canopy. *Glob. Change Biol.* **2006**, *12*, 1174–1188. [[CrossRef](#)]
72. Garrity, S.R.; Bohrer, G.; Maurer, K.D.; Mueller, K.L.; Vogel, C.S.; Curtis, P.S. A comparison of multiple phenology data sources for estimating seasonal transitions in deciduous forest carbon exchange. *Agric. For. Meteorol.* **2011**, *151*, 1741–1752. [[CrossRef](#)]
73. Melaas, E.; Friedl, M.A.; Zhu, Z. Detecting interannual variation in deciduous broadleaf forest phenology using Landsat TM/ETM+ data. *Remote Sens. Environ.* **2013**, *132*, 176–185. [[CrossRef](#)]
74. Liang, L.; Schwartz, M.D.; Fei, S. Validating satellite phenology through intensive ground observation and landscape scaling in a mixed seasonal forest. *Remote Sens. Environ.* **2011**, *115*, 143–157. [[CrossRef](#)]
75. Nijland, W.; Bolton, D.; Coops, N.; Stenhouse, G. Imaging phenology; scaling from camera plots to landscapes. *Remote Sens. Environ.* **2016**, *177*, 13–20. [[CrossRef](#)]
76. Richardson, A.D.; Hufkens, K.; Li, X.; Ault, T.R. Testing Hopkins’ Bioclimatic Law with PhenoCam data. *Appl. Plant Sci.* **2019**, *7*, e01228. [[CrossRef](#)] [[PubMed](#)]
77. Delbart, N.; Kergoat, L.; Le Toan, T.; Lhermitte, J.; Picard, G. Determination of phenological dates in boreal regions using normalized difference water index. *Remote Sens. Environ.* **2005**, *97*, 26–38. [[CrossRef](#)]
78. Snyder, K.A.; Huntington, J.L.; Wehan, B.L.; Morton, C.G.; Stringham, T. Comparison of Landsat and Land-based phenology camera Normalized Difference Vegetation Index (NDVI) for dominant plant communities in the Great Basin. *Sensors* **2019**, *19*, 1139. [[CrossRef](#)]

79. Luquez, V.M.; Hall, D.; Albrechtsen, B.R.; Karlsson, J.; Ingvarsson, P.; Jansson, S. Natural phenological variation in aspen (*Populus tremula*): The SwAsp collection. *Tree Genet. Genomes* **2007**, *4*, 279–292. [[CrossRef](#)]
80. Churkina, G.; Schimel, D.; Braswell, B.; Xiao, X. Spatial analysis of growing season length control over net ecosystem exchange. *Glob. Change Biol.* **2005**, *11*, 1777–1787. [[CrossRef](#)]
81. Migliavacca, M.; Galvagno, M.; Cremonese, E.; Rossini, M.; Meroni, M.; Sonnentag, O.; Cogliati, S.; Manca, G.; Diotri, F.; Busetto, L.; et al. Using digital repeat photography and eddy covariance data to model grassland phenology and photosynthetic CO₂ uptake. *Agric. For. Meteorol.* **2011**, *151*, 1325–1337. [[CrossRef](#)]



© 2020 by the authors. Licensee MDPI, Basel, Switzerland. This article is an open access article distributed under the terms and conditions of the Creative Commons Attribution (CC BY) license (<http://creativecommons.org/licenses/by/4.0/>).